Robotica: page 1 of 17. © Cambridge University Press 2018
doi:10.1017/S0263574718001108

Design of a robust stair-climbing compliant modular robot to tackle overhang on stairs

Ajinkya Bhole†, Sri Harsha Turlapati†, Rajashekhar V.S†, Jay Dixit†, Suril V. Shah‡* and K. Madhava Krishna†

†*IIIT Hyderabad, Hyderabad, India*
‡*Department of Mechanical Engineering, Indian Institute of Technology Jodhpur, Jodhpur, India*

(Accepted September 24, 2018)

SUMMARY
This paper discusses the concept and parameter design of a robust stair-climbing compliant modular robot, capable of tackling stairs with overhangs. Geometry modifications of the periphery of the wheels of our robot helped in tackling overhangs. Along with establishing a concept design, the robust design parameters are set to minimize performance variations. The Grey-based Taguchi method is applied to provide an optimal setting for the design parameters of the robot. The robot prototype is shown to have successfully scaled stairs of varying dimensions, with overhang, thus corroborating the analysis performed.

KEYWORDS: Modular Robot, Compliant Joint, Stair-Climbing, Overhung

1. Introduction

Stair traversal is a critical requirement for search and rescue robots as many of the terrestrial mission scenarios occur in urban settings with stairs. In this paper, we present the concept design of a stair-climbing compliant modular robot (Fig. 1), which can tackle overhangs on stairs. The robot is also equipped with robust design parameters, which make the performance of the robot insusceptible to varying step dimensions. Although legged mechanisms have shown a tremendous advantage in traversing uneven terrain and climbing over obstacles, these robots have complex designs, need advanced control strategies and suffer from a sluggish motion. A wheeled mechanism is a better option due to its design simplicity, lower power consumption and quick mobility. This justifies our choice of a wheeled robot.

Power consumption in an urban search and rescue robot is a cardinal performance factor, as the robot must not come to a stop in the middle of a mission by draining its power source. Hence, it is essential to develop energy-efficient robots for such operations. The wheel diameter is one of the major design factors, which affects the power consumption of a wheeled robot. Large wheels often become bulky, require high driving torque and thus result in greater power consumption as compared to the smaller wheels. In the following development, robots with the wheel diameter smaller than the stair riser height are referred to as "Class I" robots, and "Class II" robots the vice-versa.

Our previous works,[1–3] and the Rocker–Bogie,[4] Shrimp[5] and Octopus[6] are examples of Class I robots, while robots like Asguard,[7] Genbu,[8] Rhex,[9] Impass[10] and Loper[11] are Class II robots. Robots with tracked wheels have also existed in the past.[12] Although Class I robots have the advantage of low power consumption over Class II robots, Class I robots suffer from the drawback that their mechanisms have a possibility of getting jammed under a step overhang (as explained in Section II). Overhangs are protrusions beyond the face of the stair riser on the front edge of a stair. Class II robots owing to their larger wheels do not face this problem as they are able to make direct contact with the vertical

* Corresponding author. E-mail: surilshah@iitj.ac.in

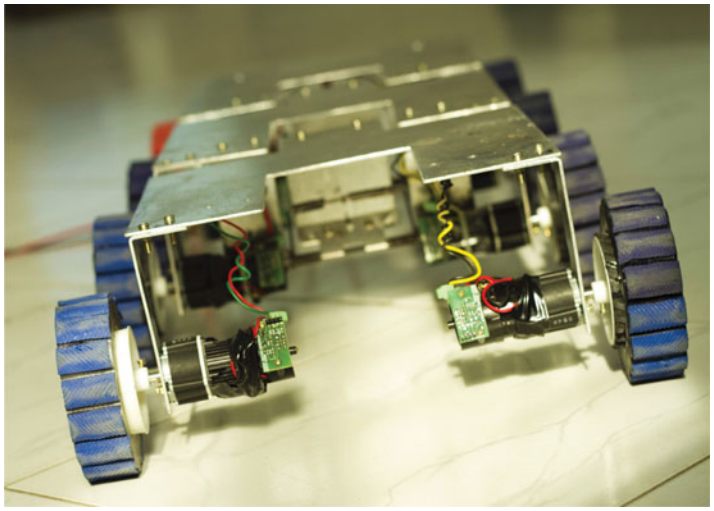

Fig. 1. Stair-climbing compliant modular robot prototype.

face of the overhang or the next step tread. To the best of our knowledge, this drawback of Class I robots has not been addressed in any previous works on stair-climbing robots. This work undertakes the problem of overcoming overhangs by keeping intact the feature of Class I robots, i.e., having a wheel diameter less than that of the stair riser height (less than three-fourths of the stair riser height to be precise). This provides the advantage of low power consumption. This endeavor was achieved by modifying the design of the wheels of the robot by blending equally spaced circular arcs on the periphery of the wheels.

As mentioned earlier, we also design the robot with robust design parameters so that its performance is least affected due to varying step dimensions. For a robust design of the robot, we define desired performance metrics that depend on certain critical controllable and uncontrollable design parameters. We consider the overall power consumed by the robot as one of the performance metrics. It depends on the controllable design parameters, namely, the length of the module, radius of the wheel and number of arcs on the wheel, and among the uncontrollable design parameters are the varying stair dimensions and the coefficient of friction. The wheel design modification of integrating arcs on the periphery of the wheel introduces transverse alterations in the path of the robot. Thus, along with the overall power consumption, we also set the amplitude and frequency of the transverse alterations as the performance metrics. Altogether, we set the controllable design parameters such that the power consumption and its variation, and the amplitude and frequency of transverse alterations arising from the wheel design modification are reduced. For this, the Grey-based Taguchi method,[13–16] a multi-objective optimization method, is used that takes care of the robustness as well as combining multiple performance attributes together for the decision-making process to obtain an optimal set of controllable design parameters. Earlier designs have also turned to multi-objective optimization methods to decide on several design parameters.[17]

A body of work has been devoted to the concept design of robots for stair climbing, but none of them discussed specifically on the challenge of tackling overhangs with a rigor like ours to the best of our knowledge. This provides a novelty to our work. Also, many previous works on stair-climbing robots have considered random stair dimensions or dimensions that suit their robot designs for the purpose of analysis. The proposed work, on the other hand, considers stair dimensions that follow the International Building Code (IBC)[18] providing it a high impact for rescue operations in urban settings.

Our previous work[3] detailed the design methodology for approximating the optimal spring stiffnesses required by a multi-modular wheeled robot to climb stairs in a quasi-static manner. The same work also provided results validating the robustness of the designed robot in climbing different types of stairs. In contrast to the design of our previous robot,[3] this work contributes as follows. First, a solution to overcome overhang is proposed by modifying the wheel design systematically. Second, it poses the parametric design of the robot as a multi-objective optimization problem. Since

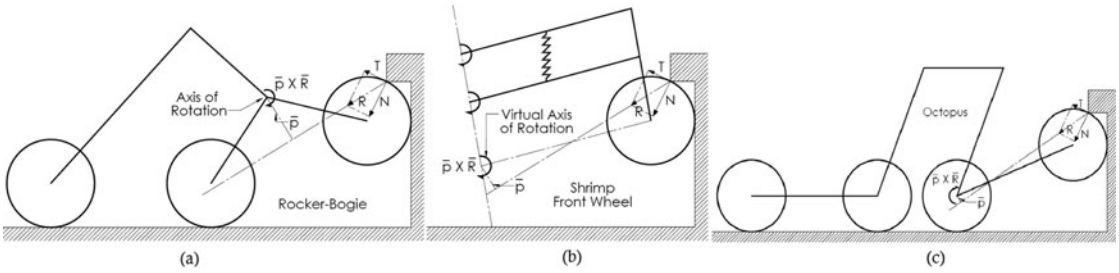

Fig. 2. Some eminent Class I robots that could get jammed under stair overhang.

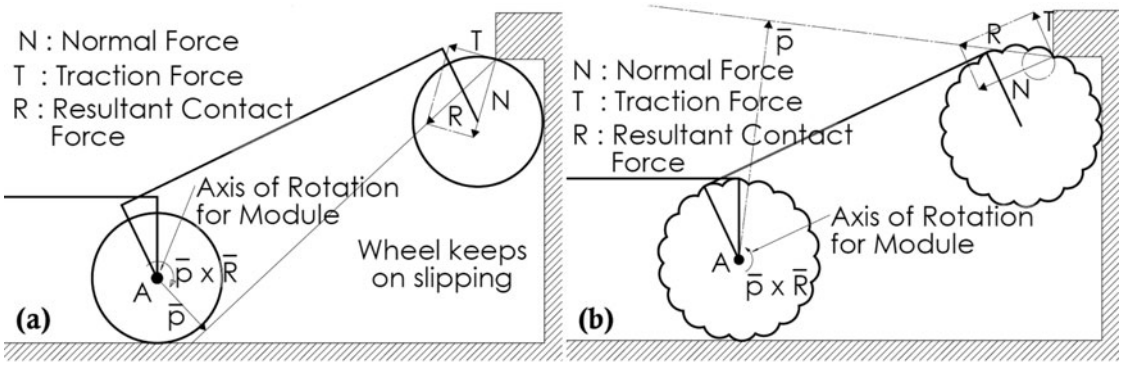

Fig. 3. (a) Circular wheel failing to provide the desired counter-clockwise moment about the axis of rotation for module. (b) Modified wheel design providing the desired counter-clockwise moment.

a functional characterization of the same is almost intractable, it makes use of statistical methods[13–16] to solve for the optimal design. Setting the range for the design factors for this optimization problem forms a cardinal part of this work. This is a critical job, as setting an arbitrary range can lead to some configurations in which the robot can get stuck or even not climb. With a careful analysis of all design factors, we have logically backed every design factor's range selection. As a consequence of this design procedure, a prototype was fabricated and was shown to climb stairs and overhangs of varying dimensions. To the best of our knowledge, such a formal method of posing wheel design to tackle overhangs as a statistical optimization formulation and the concomitant analysis and detailed experimental verification does not appear in the surveyed literature.

The paper is organized as follows: Section 2 discusses a concept design for tackling overhangs on stairs. A model for the parametric design of the robot is set up in Section 3. Section 4 presents design of experiments for evaluating performance metrics through Taguchi's Orthogonal Array (OA) experiments. Section 5 confirms the analysis performed by practical experimentation. Finally, conclusions and scope of future work are discussed in Section 6.

2. Concept Design

The previous design of our stair-climbing compliant modular robot[3] with wheels of diameter less than the stair riser height got jammed under the overhangs, as shown in Fig. 3(a). In Fig. 3, $\bar{p}$ is the vector going from the center of the wheel to the resultant contact force $\bar{R}$. Here, the first module gets jammed under the overhang as the external contact force $\bar{R}$ obtained from the ground on the wheel fails to provide a counter-clockwise moment about the axis of rotation of the module, i.e., axis A. This prevents the module from folding inwards and thus disables climbing. As evident from Fig. 2, the similar problem would also be faced by some of the other eminent Class I robots.

A counter-clockwise moment can be easily achieved by changing some of the design parameters of the robot. For example, decreasing the length of the module and increasing the radius of the wheel to such an extent that the contact force starts providing the desired counter-clockwise moment are viable options. However, as discussed in Section III(C-b), in our case, the module length is constrained by a certain lower bound, reducing which the module tips over while climbing. Increasing the radius of

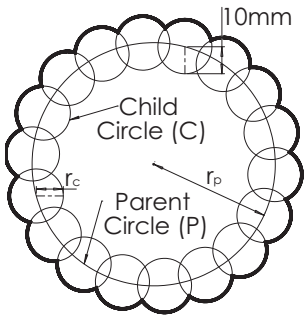

Fig. 4. Wheel design.

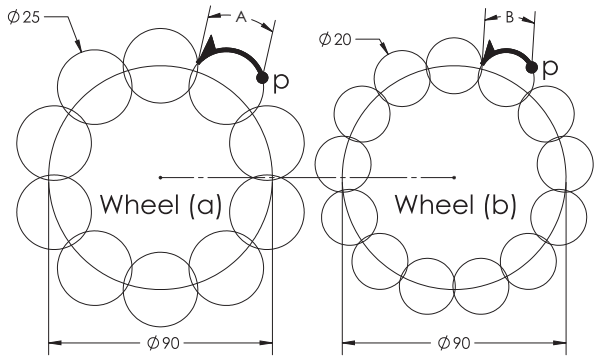

Fig. 5. Child circle size selection.

the wheel is also an unfavorable option, as this makes the robot quite bulky and increases the power consumption. Similar design constraints can also occur in other Class I robots.

The exercise of integrating knowledge of the geometry of stairs and mechanical interaction into a solution to the stair-climbing problem usually comes in one of two flavors: one can either use design enhancements[3–5] or generate plans (e.g., Rhex[9] uses a special algorithm). The wheel shape is an easily alterable design freedom with potential benefits both in terms of simplicity and robustness; hence, we explored this. We modified the wheel design of our robot. Circular arc geometry, instead of spiky geometry, is chosen on the periphery of the wheel as it ensures a gradual variation in the direction of the contact force from the ground. This, consequently, avoids undesired fluctuations in the torque required from the motor. As can be seen in Fig. 3(b), blending arcs on the circumference of the wheel changes the direction of the resultant contact force obtained from the overhang, providing a counter-clockwise moment about the axis of rotation of the folding module.

As shown in Fig. 4, the wheel is designed by drawing a parent circle P of radius r_p and evenly spaced child circles C of radius r_c on the circumference of the parent circle. Varying the radius of parent circle and the number of child circles changes the shape of the circumference of the wheel. The criterion for the selection of the child circle size is detailed ahead. Figure 5 shows designs of two different wheels with different radii for child circle (Wheel (a) with a greater radius). The radius of the parent circle was kept the same for both the wheels, and the number of child circles was set to a minimum value so as to not allow the child circles to be disjointed. This condition is explicated in Section III(C-c). If for both the wheels, a point p on the child circle contacts the lower tip of the overhang where slippage starts occurring due to the inability of the contact force to produce counter-clockwise moment about axis of rotation of the module, then Wheel (a) will take a greater time to come out of this slippage. This is because Wheel (a) needs to cover a greater arc length (A>B) before coming to a point on the wheel periphery that ends slippage. Hence, it is better to keep the radius of the child circle as low as possible.

However, for the practical purpose, this radius cannot be set too low. This is because wheels usually require a rubber covering over them, helping them to get a good traction over the surface to be travelled. Setting child circle radius too low will result in the rubber covering the child circle shape.

Such geometry would, in fact, become almost circular and thus resemble a normal circular wheel that fails in overcoming overhang. Thus, we set a reasonable diameter for the child circle, one which is comparable with the dimension of the overhang and fixed its value to 20 mm. This reduces the number of variables, which results in the changing wheel geometry and, thus, lowers the design complexity.

Eminent robots like Asguard[7] and Whegs[19] also have adopted the strategy of change in the wheel design to tackle stairs. As opposed to their design, we have tried to keep the wheel as close to a circle as possible. This provides a greater amount of contact with the ground, thus better traction, speed and low power consumption. In order to demonstrate reduction in the power consumption, we fitted the robot with the wheel designs used in refs. [7] and [19], keeping the same outer diameter. We ran simulation experiments and measured the power consumption for a run with the constant motor speed of 10 rpm on a flat terrain for 5 s. It was observed that the wheels mentioned in refs. [7] and [19] consumed 0.3252 W and 0.8516 W, respectively, while the robot with the proposed wheel design consumed 0.1544 W, thus clearly showing the superiority of the proposed wheel design. Along with the low power consumption, the robot also traversed a longer distance due to the greater circularity of wheels, thus showcasing its efficacy.

3. Parameter Design

The multiple performance goals of increasing the robustness of the robot and reducing the transverse alterations that result from the wheel design can be achieved by setting up a proper model for the parametric design. Posing this as an optimization problem to solve for the optimal parameters is quite difficult owing to the complexity of the design. Statistically evaluating the performance based on different experiments intuitively points in the direction of the optimal design choices. This is achieved using the Grey-based Taguchi method, a widely adopted statistical method for solving Multiple Attribute Decision Making problems.[13–16] This method is a combination of the Taguchi method[20] and the Grey Relational Analysis (GRA).[21] The Taguchi method provides a robust design for the robot, while the GRA helps in combining various performance metrics into a single metric for decision making.

The Grey-based Taguchi method involves defining the desired performance metrics (response) and the various controllable and uncontrollable (noise) factors and their levels in the system, influencing the defined performance metrics. These performance metrics and the design factors are discussed in the immediate subsections.

The notations and their meaning used in this section are explained in Table I.

3.1. Performance attributes

While deciding the performance attributes, it may be noted that reducing vibrations is equally important as it helps in acquiring less noisy data from the on-board sensors.[22] Therefore, the power consumed by the eight motors of the robot in climbing four steps (p_r), the amplitude (a_t) and frequency of transverse alterations (f_t) are considered as the performance attributes. From Fig. 6, a_t is given by

$$a_t = B - A = r_p(1 - \cos(\delta/2))$$

The frequency of transverse alterations per rotation of the wheel is equal to the number of child circles on the wheel:

$$f_t = n_c$$

3.2. Noise factors

The factors affecting the performance of a system, which are beyond the control of the designer, are termed as noise factors. The Grey-based Taguchi method provides a design setting, making the performance of the system least sensitive to these factors. The coefficient of friction and the varying stair dimensions are the noise factors in our system. We consider three different stair dimensions as shown in Fig. 7, which follow the IBC. For the simplicity of analysis, we assumed the coefficient of friction to be constant.

Table I. Notations and their meanings.

Notation	Meaning
r_c	Radius of child circle
r_p	Radius of parent circle
p	Point on the child circle in contact with the lower tip of the overhang where wheel slippage starts to occur
p_r	Power consumed by the robot
a_t	Amplitude of transverse alterations
f_t	Frequency of transverse alterations
δ	Angle inscribed by the center of two child circles placed side by side
$o_{\max}$	Maximum overhang dimension
$o_{\min}$	Minimum overhang dimension
$\text{riser}_{\min}$	Minimum riser dimension
$\text{tread}_{\min}$	Minimum tread dimension
l_m	Length of module
L_{up}	Upper bound on the length of the module
n_c	Number of child circles
n_{lb}	Lower bound on the number of child circles
n_{up}	Upper bound on the number of child circles
ϕ_1	Angle made with the horizontal by the line joining the center of the climbing wheel and the center of its child circle touching the face of the riser
ϕ_2	Angle between the line joining the lower tip of the overhang with the center of the child circle climbing the overhang and the line joining the center of the same child circle with the center of the parent circle
ϕ_3	Angle made by the line joining the center of the second wheel on the ground and the lower tip of the overhang with the horizontal
ϕ_4	Angle made by the normal reaction force obtained from the overhang with the horizontal
p_n	Number of angles, δ, inscribed by the lines joining the center of the parent circle and the centers of the child circle touching the face of the riser and the child circle touching the lower tip of the overhang
c	Module clearance
k_i^+	Stiffness values of the springs at the ith joint opposing the counter-clockwise moment on a module
k_i^-	Stiffness values of the springs at the ith joint opposing the clockwise moment on a module

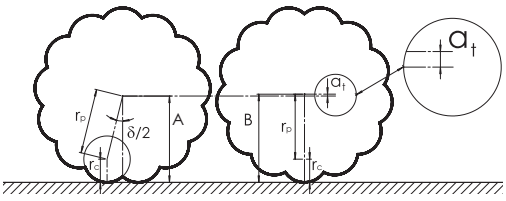

Fig. 6. Geometry for calculating amplitude of transverse alterations.

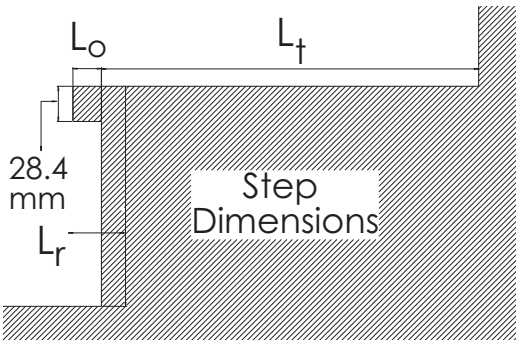

	Length of Overhang L_o(mm)	Length of Riser L_r (mm)	Length of Tread L_t (mm)
Step 1	23	177.8	304.8
Step 2	25	190.5	292.1
Step 3	27	203.2	279.4

Fig. 7. Varying step dimensions.

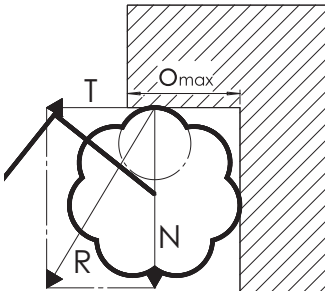

Fig. 8. Concept for setting the lower bound on the radius of the parent circle: Normal force acting vertically downwards.

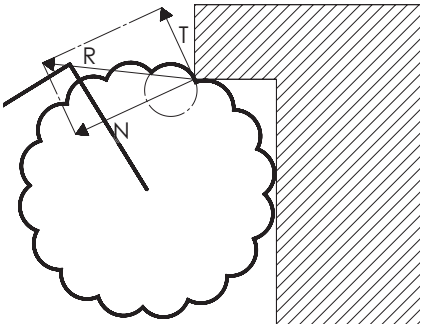

Fig. 9. Concept for setting the lower bound on the radius of parent circle: Normal force shifted clockwise towards the axis of rotation of module.

3.3. Control factors

Control factors are the design parameters that can be practically controlled. It is necessary to identify the factors that influence the performance of the system. Successful climbing of the robot is necessary to analyze the performance. A climb is considered successful when the robot is able to traverse the stairs without getting stuck in certain configurations or under the overhang. The optimization problem will thus have a solution space only for successful climbs. Choosing appropriate ranges of the control factors is thus necessary so as to leave out the unfeasible solution space. The various control factors and their ranges are described ahead.

Parent radius of wheel (r_p): Small-sized wheels create problems in geometrical trafficability of the robot. In the case of a wheel radius lesser than the overhang dimension, the normal reaction force obtained from the overhang acts vertically downwards, as depicted in Fig. 8. Keeping the radius greater than the overhang dimension shifts the normal force from a vertically downward direction towards the axis of rotation of module. This is illustrated in Fig. 9. This makes it easier for the resultant contact force to provide a counter-clockwise moment about the axis of rotation of module. Therefore, the lower bound of the overall radius of the wheel was set as the maximum overhang length allowed according to the IBC standards.

Many of the stair-climbing robots usually make use of large wheels with a diameter greater than the step riser dimensions.[7–11] This makes the robot bulky, thus consuming enormous power. Taking this into consideration, we undertook the challenge of stair climbing and tackling overhangs with wheels smaller than step riser. We set the upper bound on the overall wheel diameter as three-quarters of the minimum riser dimension considered in our analysis. This gave us the following range for the levels for the parent radius:

$$\begin{aligned} r_p + r_c &\geq o_{\max} \\ 2(r_p + r_c) &\leq \frac{3}{4}(\text{riser}_{\min}) \\ 21.25 \text{ mm} \leq r_p &\leq 56.67 \text{ mm} \end{aligned} \tag{1}$$

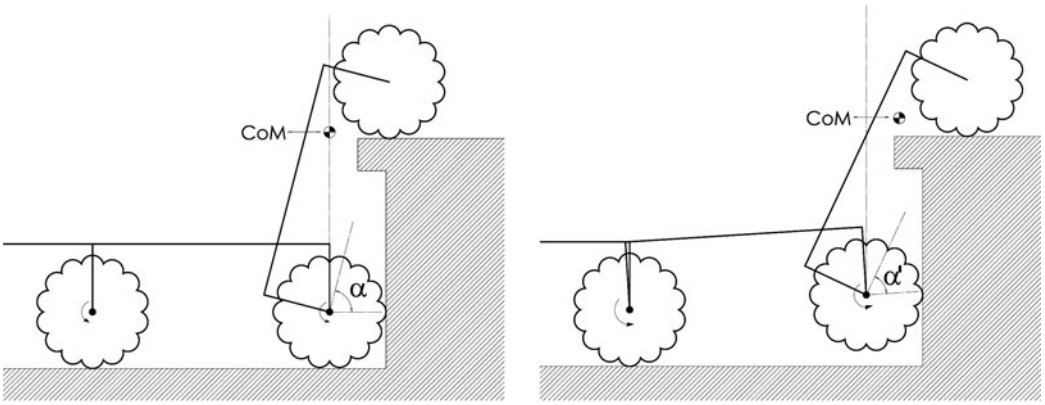

Fig. 10. Concept for setting a lower bound on the module length.

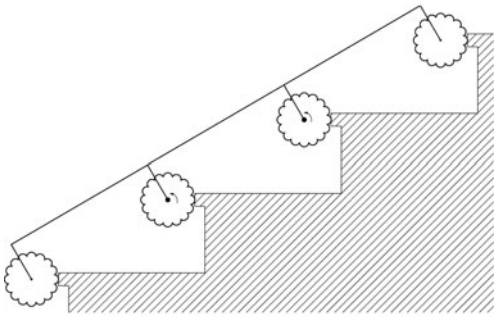

Fig. 11. Concept for setting an upper bound on the module length.

here, $o_{\max} = 31.75$ mm is the maximum overhang dimension allowed according to the IBC, $\text{riser}_{\min} = 177.8$ mm is the minimum step riser dimension considered in our analysis and r_c is the child circle radius of the wheel.

Length of module (l_m): As discussed in our previous work,[1] the first module climbs a step until it crosses a limiting angle, in which case the module tips over. This occurs because the center of mass of the module, climbing up the stair, starts generating a counter-clockwise moment about the axis of rotation of the module. As can be seen in Fig. 10, the length of the module is kept in such a way that the center of mass of the climbing module generates clockwise moment about its axis of rotation, until its wheels overcome the overhang and contact the stair tread. This assuredly avoids tip over, as after this, the relative angle α between the first and the second module starts decreasing subsequently. The lower limit for the length of the module was set considering this requirement. Calculation of the position of the center of mass of the module requires the length of the module itself. Hence, to find this lower limit, an iterative procedure was used by gradually changing the length of the module from a smaller to a higher value and checking through simulation if the module is able to climb the overhang.

For a certain range of the module length, configurations similar to the one shown in Fig. 11 arise. Such a configuration is undesirable because there are no contact forces pushing the robots forward on the stairs. For this reason, at least one set of the wheels must be present on the step tread, so that they are able to push/pull the other wheels on the step riser. This can be achieved by setting the length less than the one shown in Fig. 11. The upper bound on the length of module L_{up} thus has to satisfy the following equation:

$$L_{\text{up}} \leq \sqrt{(o_{\min}^2 + \text{tread}_{\min}^2) + \text{riser}_{\min}^2} \tag{2}$$

where $o_{\min}$, $\text{tread}_{\min}$ and $\text{riser}_{\min}$ are the minimum dimensions of the overhang, tread and the riser considered in our analysis, respectively.

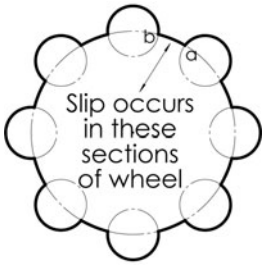

Fig. 12. Concept for setting a lower bound on the number of child circles.

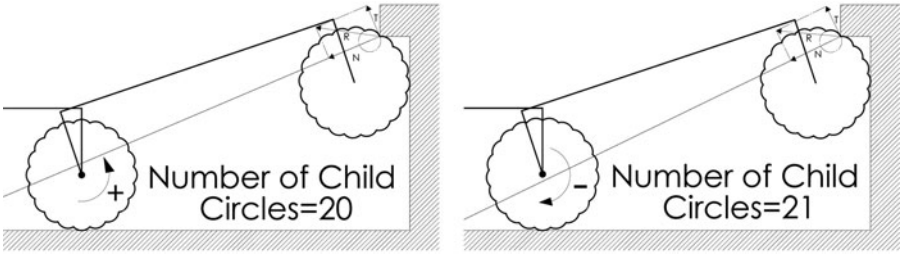

Fig. 13. Concept for setting an upper bound on the number of child circles.

The following range was obtained for the module length considering these requirements:

$$210.96 \text{ mm} \leq l_m \leq 352.37 \text{ mm} \tag{3}$$

Number of child circles (n_c): As illustrated in Fig. 12, the lower bound n_{lb} for the number of child circles was chosen such that the parent circle does not occupy any part of the circumference of the wheel, i.e., by not allowing the child circle to be disjointed. This is because wheel slip occurs on the sections on the circumference occupied by the parent circle while on the overhang. This measure does not completely cancel the slippage but reduces it. Reducing slip is important since having repeated slipping as the robot climbs stairs is going to cause more energy consumption. The condition for lower bound can be given as follows:

$$n_{\text{lb}} = \lceil x \rceil \quad s.t. \quad x(2r_c) = 2\pi r_p$$

Figure 13 depicts that with the increase in n_c, the moment generated due to the normal reaction gradually becomes clockwise from counter-clockwise. The supremum for the number of child circles n_{up} was chosen, such that the normal reaction obtained from the overhang generates a counter-clockwise moment about the axis of rotation of the module, as can be seen in Fig. 14. This assures that even with minimal coefficient of friction, the resultant contact force R generates a counter-clockwise moment. These conditions are contained in the following optimization:

$$\begin{aligned}
&\text{Maximize} \quad n_{\text{up}} \\
&\text{Subject to} \\
&\qquad \text{(i)} \ (\phi_1, \phi_2, \phi_3, \phi_4, \delta) \in \mathbb{R} \\
&\qquad \text{(ii)} \ (n_{\text{up}}, p_n) \in \mathbb{Z}^+ \\
&\qquad \text{(iii)} \ r_p \cos(\phi_1) + r_c = r_p \cos(\phi_1 + p_n\delta) \\
&\qquad\qquad\qquad\qquad + r_c \cos(\phi_1 + p_n\delta - \phi_2)
\end{aligned}$$

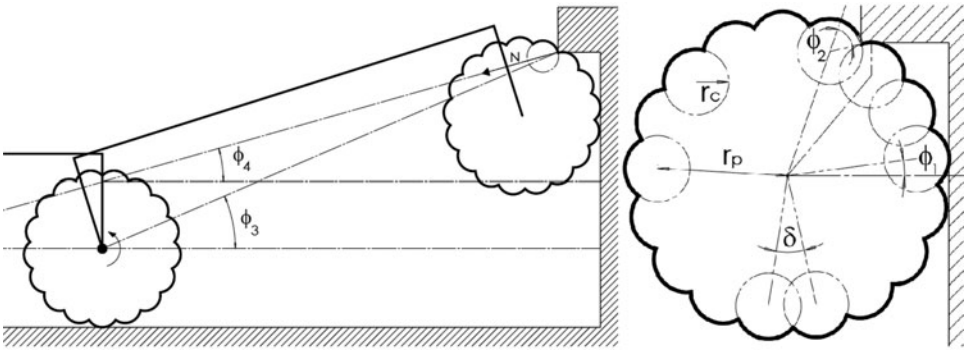

Fig. 14. Geometry for setting an upper bound on the number of child circles.

$$\text{(iv)}\ r_p \sin(\phi_1 \pm \delta) + r_c \leq r_p \cos(\phi_1) + r_c$$

$$\text{(v)}\ r_p \sin(\phi_1 + (p_n - 1)\delta) + r_c = r_p \sin(\phi_1 + p_n\delta) + r_c \sin(\phi_1 + p_n\delta - \phi_2)$$

$$\text{(vi)}\ -\left(\frac{\delta}{2}\right) < \phi_1 \leq \left(\frac{\delta}{2}\right)$$

$$\text{(vii)}\ 0 \leq \phi_2 \leq \left(\frac{\delta}{2}\right) + \sin^{-1}\left(\frac{r_p \sin(\frac{\delta}{2})}{r_c}\right)$$

$$\text{(viii)}\ p_n \leq \left\lceil \left(\frac{n_{\text{up}}}{4}\right) \right\rceil$$

$$\text{(ix)}\ \phi_4 \leq \phi_3$$

where ϕ_1 is the angle made with the horizontal by the line joining the center of the climbing wheel and the center of its child circle touching the face of the riser, as shown in Fig. 14. ϕ_2 is the angle between the line joining the lower tip of the overhang with the center of the child circle climbing the overhang and the line joining the center of the same child circle with the center of the parent circle. ϕ_3 is the angle made by the line joining the center of the second wheel on the ground and the lower tip of the overhang with the horizontal. ϕ_4 is the angle made by the normal reaction force obtained from the overhang with the horizontal. δ is the angle inscribed by the lines joining the center of the wheel and any two consecutive child circles. p_n is the number of angles. Constraints (i) and (ii) represent the domain of the variables, (iii)–(v) are the geometrical constraints, (vi)–(viii) contain the range of the variables and constraint (ix) ensures that the normal reaction force generates the desirable counter-clockwise moment. Considering these bounds, the following range was obtained for the number of child circles:

$$16 \leq n_c \leq 20 \tag{4}$$

For the simplicity of the analysis, the control variables, clearance c between the ground and the module link, and the stiffness values of the springs at the joints were kept constant. In order to ensure geometrical trafficability, clearance c was set considering that it is maximum when the wheel size is minimum and the module link length is maximum with an additional safety margin.[1]

The stiffness values for the springs at the joints, for all possible combinations of the control factors, are calculated as explained in the appendix. A mean value was considered for the purpose of analysis. Following are the values considered for the clearance and the spring stiffness at the joints:

- $c = 100$ mm
- $k_1^+ = 74.47$ N mm/deg $\quad k_1^- = 67.56$ N mm/deg
- $k_2^+ = 48.89$ N mm/deg $\quad k_2^- = 57.61$ N mm/deg

Table II. Orthogonal Array $L_9(3^3)$ experiments and their results.

Run no.	A	B	C	Power required to climb 4 steps (W) p_1^r	p_2^r	p_3^r	*S/N* ratio	Amplitude (mm)	Frequency
1	1	1	1	4.02	4.07	5.19	−12.98	0.76	16
2	1	2	2	3.12	3.47	3.35	−10.43	0.68	18
3	1	3	3	3.49	3.87	3.79	−11.42	0.61	20
4	2	1	2	2.96	2.90	3.52	−9.95	0.60	18
5	2	2	3	2.99	2.99	3.08	−9.61	0.55	20
6	2	3	1	3.57	3.36	3.61	−10.93	0.96	16
7	3	1	3	4.28	3.95	3.70	−12.01	0.49	20
8	3	2	1	3.33	2.90	3.44	−10.19	0.86	16
9	3	3	2	3.96	3.41	4.15	−11.72	0.75	18

Note: A: Levels of module length; B: Levels of radius of parent circle; C: Levels of number of child circles; p_i^r is the power consumed by robot on the *i*th stair dimension.

where k_i^+ and k_i^- are the stiffness values of the springs at the *i*th joint opposing the counter-clockwise and the clockwise moments, respectively.

Three levels are set for each control parameter taking into consideration Eqs. (1)–(4). The levels, Level 1, Level 2 and Level 3, set for the module length are 240 mm, 260 mm and 280 mm, that for radius of the parent circle are 40 mm, 45 mm and 50 mm, and finally for the number of child circles are 16, 18 and 20, respectively.

4. Design of Experiments

An all-inclusive experimentation of the control and noise factor levels under study would have required 81 experiments. Taguchi's OA[20] provides a condensed set of experiments, which are balanced to ensure that all levels of factors are considered equally and can be evaluated independently of each other. Based on the number of parameters and their levels, the present experimentation was designed as per Taguchi's $L_9(3^3)$ OA. It is quite time consuming, tedious and uneconomical to conduct physical experiments for all the combinations in the OA. For this reason, we simulated our experiments in *SolidWorks Motion Analysis*, which is a robust physics-based solver. A similar approach of using simulation in Taguchi's method can be seen in refs. [23–25]. The subsections ahead describe the experiments and the analysis performed on the experimental results.

4.1. Performance metrics and their data collection

Robustness can be achieved by identifying control factors that reduce variability in a product/process, and by minimizing the effects of uncontrollable factors (noise factors). Noise factors cannot be controlled during actual usage of product but can be controlled during experimentation. In Taguchi-based design of experiments, noise factors are manipulated to force variability to occur and from the results, and to identify optimal control factor settings that make the process or product robust or resistant to variation from the noise factors. Here, we vary the stair dimensions to force variability in the performance metrics.

The performance values collected from each run in the OA are tabulated in Tables II and III. The signal to noise ratio (*S/N*), which reflects the ability of the system to perform well in the presence of noise factors, is considered as the metric for the power consumption attribute. It may be noted that *S/N* ratio is not required for the amplitude and frequency attributes as they do not change with the varying stair dimensions. As the objective is to minimize the power consumption, the "smaller-the-better" formula for *S/N* ratio given below is used:

$$S/N \text{ ratio} = \eta = -10 \log_{10} \left[\frac{1}{n} \sum_{i=1}^{n} (p_i^r)^2 \right]$$

Table III. $L_9(3^3)$ Grey relational coefficients, Grey grades and rank.

Run no.	A	B	C	Grey relational coefficients			Grey relational grade	Rank
				Power	Amplitude	Frequency		
1	1	1	1	0.33	0.45	0.86	0.59	5
2	1	2	2	0.67	0.55	0.79	0.57	7
3	1	3	3	0.48	0.65	0.72	0.49	8
4	2	1	2	0.83	0.67	0.71	0.66	3
5	2	2	3	1	0.79	0.64	0.70	2
6	2	3	1	0.56	0.33	1	0.63	4
7	3	1	3	0.41	1	0.55	0.58	6
8	3	2	1	0.74	0.38	0.94	0.70	1
9	3	3	2	0.44	0.46	0.86	0.47	9

Table IV. Influence of control parameters on Grey relational grade.

Control parameter	Average Grey relational grade by factor level		
	Level 1	Level 2	Level 3
Module length	0.554162	0.668827*	0.587269
Radius of parent circle	0.615386	0.664180*	0.530693
Number of child circles	0.646039*	0.570653	0.593566

Optimal levels are indicated by symbol*.

where η denotes the S/N ratio calculated from the obtained p_i^r's that are the power consumption values from the ith run in the OA. n is the number of times an experiment in the OA is repeated, and is equal to the levels of noise factors, here, 3.

4.2. Multi-attribute decision-making method

GRA,[21] a multi-attribute decision-making technique, is used to obtain the optimum set of various input parameters for the best performance characteristics. GRA first, translates performance of all alternatives into a comparability sequence, a normalized data sequence between 0 and 1. Following the normalization, Grey relational coefficients (GRC) are calculated to express the relationship between the ideal and normalized data sequence. A distinguishing coefficient is used to expand or compress the range of the GRC. We calculated the GRC considering a distinguishing coefficient of 0.5. The Grey relational grade for each combination of the control factors in the OA was obtained by preferential weighing of their GRC, i.e., by giving precedence to the power consumption. The experiments were then ranked according to their Grey relational grades. Table III tabulates these results.

The influence of each control parameter on the Grey relational grade is presented in Table IV, providing the following optimal setting:

- Module length = 260 mm,
- Radius of parent circle = 45 mm and
- Number of child circles = 16

4.3. Explanation of the Grey relational analysis results

In all the simulation experiments, the angular velocity of all the wheels was kept constant. Therefore, the power consumed by the robot is in proportion to the torque provided by the motors. As the wheel radius increases, the required driving torque also increases, thus increasing the power consumption. According to this argument, the minimum radius of the parent circle, i.e., 40 mm, should have been the optimal setting. It is worth noting that as the radius of the parent circle decreases, it becomes more difficult for the contact force on the wheel to provide a counter-clockwise moment about the axis of rotation of the module while overcoming the overhang. Hence, neither the least and nor the largest level but the nominal level of the parameter performed optimally. Same was the case with the

Table V. Analysis of variance.

	Module length	Radius of parent circle	Number of child circles	Error
Sum of squares	0.020896	0.027373	0.008962	0.001618
F-test	12.91703	16.9208	5.539721	
Percentage contribution	35.50825	46.5144	15.2284	2.748948

Table VI. Optimal setting confirmation.

		Optimal setting	
Level	Best OA expt. $A_3B_2C_1$	Prediction $A_2B_2C_1$	Simulation $A_2B_2C_1$
Power consumption			
S/N ratio	−10.1992		−9.4244
Amplitude	0.864662		0.864662
Frequency	16		16
Grey relational Grade	0.709478	0.729588	0.795383

module length. Increasing the length of the module results in configurations that enable more number of wheels to be in contact with the step tread providing a better pushing and pulling force against the step risers on the wheels climbing the risers. But, at the same time, the increase in the module length also results in an increased power consumption. Thus, a nominal value for the module length resulted as the optimal setting. As the number of child circles decreases, the normal force obtained from the overhang gets directed farther away from the axis of rotation of the module, thus making it easier for the module to overcome the overhang. Hence, the least value for the number of child circles resulted in the optimal performance.

4.4. Analysis of variance

The variability in the response variable, among different factors, is decomposed using a statistical tool, analysis of variance.[26] The F-test[26] was used to study the statistically significant control factors in our analysis. The results of the test are presented in Table V and indicate that the radius of the parent circle and the length of the module play a significant role statistically in the performance measure of the vehicle.

4.5. Prediction of Grey relational grade

The Grey relational grade can be predicted for the optimal setting using the following equation:

$$\gamma_p = \gamma_m + \sum_{i=1}^{n} (\gamma_m - \gamma_i) \tag{5}$$

where γ_p is the predicted Grey relational grade for the optimal setting, γ_m is the mean Grey relational grade, n is the number of statistically significant factors affecting the performance and γ_i is the maximum average Grey relational grade of a level for the ith statistically significant factor. The application of this to our case is presented in the immediate subsection.

4.6. Confirmation in simulation

A simulation experiment was performed at the optimal setting of the control factors. Next, Grey relational grade was calculated and compared with the predicted Grey relational grade, the results of which are tabulated in Table VI. Its closeness to the predicted grade successfully validates our analysis.

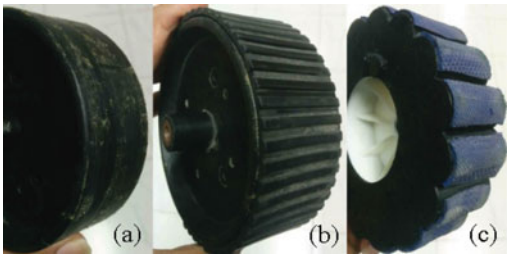

Fig. 15. The different wheels experimented with to check the climbing ability.

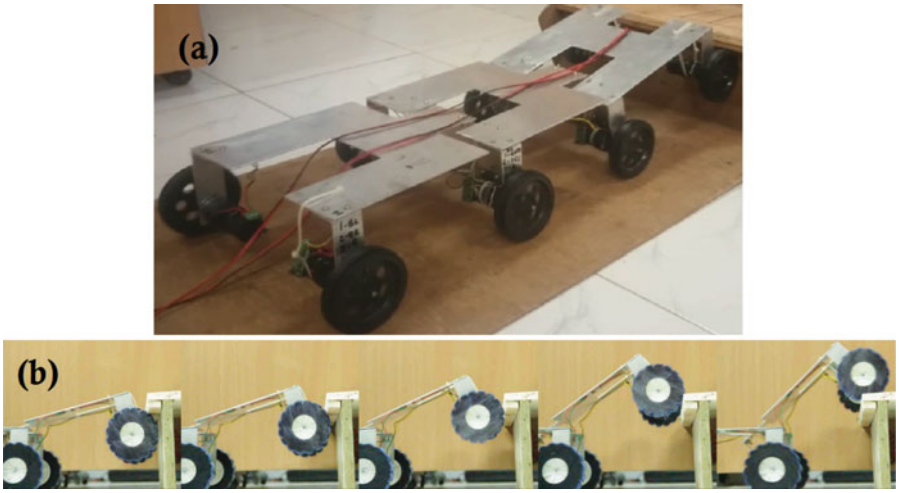

Fig. 16. (a) The robot prototype with circular wheels getting jammed under the overhang. (b) The modified wheel tackling an overhang owing to the circular arcs on the periphery.

5. Confirmation in Experiment

A robot prototype with the set of optimal design parameters obtained from the proposed framework was manufactured. The material of choice for the chassis was aluminum to cater to low weight, and the wheels were 3D printed. The wheels were rubber padded for improved traction while climbing. Compliance was added by attaching a set of torsion springs at each module joint. The motors were chosen such that they provide enough torque to achieve the desired moments for the modules to fold with respect to each other and to carry the robot's body upward to climb upstairs.

The robot equipped with a normal circular wheel with smooth rubber padding (Fig. 15(a)) failed to climb the stairs with overhang, as shown in Fig. 16(a). As discussed in Section 2, the robot fitted with wheels with low child circle radius (Fig. 15(b)) also kept on slipping at the overhang, as the rubber gets deformed and fails to provide the desired counter-clockwise moment. Figure 16(b) shows the modified wheel (Fig. 15(c)) overcoming an overhang, thus validating our concept design. The robot successfully climbed the stair dimensions considered in the analysis as well as the staircases in an urban setting without getting jammed under the overhang or getting stuck in any configuration (Fig. 17). We have even developed a standalone version of this prototype equipped with batteries, which can independently climb stairs. Its performance is captured in the form of a video and can be seen at `https://youtu.be/UKUzvtM_khY`.

The experiments involved using Faulhaber Coreless 17-W Encoder Motors for driving the robot. For the standalone version, 3 LiPo batteries were used to provide 2-A per motor pair on each module. Arduino-based controller was used to control the motors, and a remote control switch was used to turn the robot on and off and also to direct it to move around.

6. Conclusions and Future Work

In this paper, we addressed the challenge of overcoming overhang for Class I robots with wheel diameter less than the step riser dimension. The problem was tackled by introducing a systematic

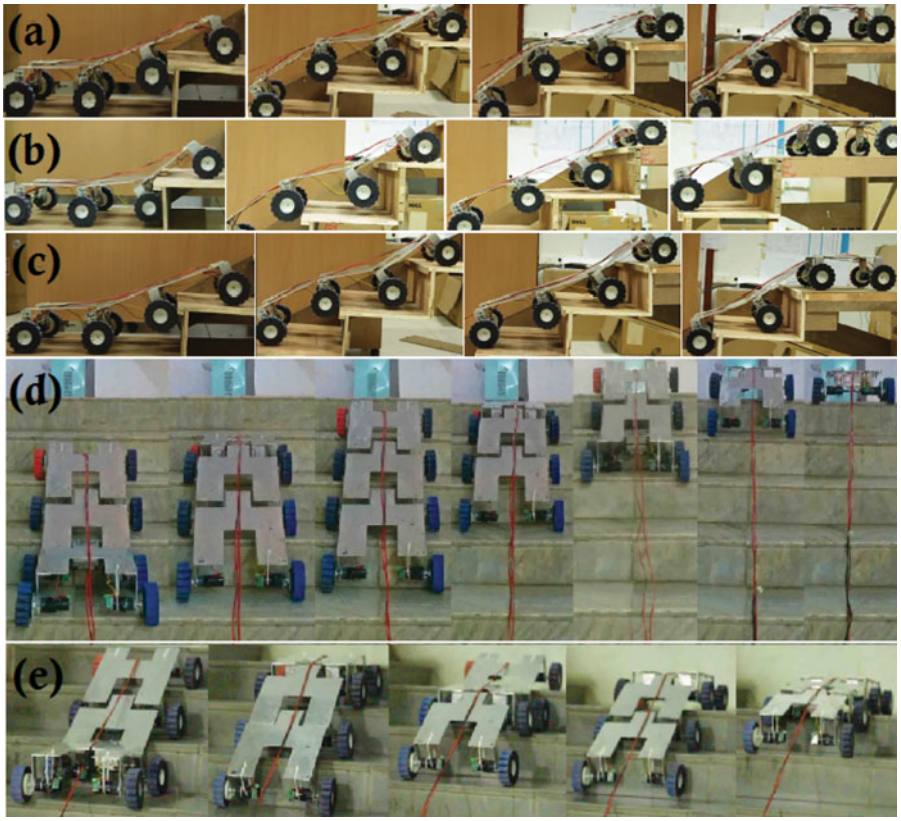

Fig. 17. The robot prototype with an optimal set of design parameters successfully climbing stairs of dimensions specified in the first, second and third levels of noise factors ((a),(b) and (c)), and on staircases in an urban setting ((c) and (d)).

modification in the wheel design. The rigorous analysis and the kind of formulation of wheel design as an optimization problem have not been proposed earlier. The chosen robust design parameters enable the robot to climb stairs of varying dimensions and make its performance least susceptible to this variation. It was concluded that it is practical to use a statistical method to obtain an optimal solution for the complex design problem in comparison to posing it as a computationally expensive non-linear optimization problem.

The varying stair dimensions considered in our analysis accord with the IBC, thus providing a high impact work for urban search and rescue operations. Simulation and experimental results corroborate the analysis performed as the robot was able to scale numerous overhang stairs with varying step dimensions.

The proposed robot design may not be able to climb successfully if the stair and overhang dimensions vary a lot from the ones considered in the paper. Another limitation of the robot is that it can turn, but only through skid steering of the wheels. We would focus our future work on developing actively controlled joints for a modular robot. Furthermore, we wish to add joints to enable the robot to turn and consequently climb circular stairs and extremely non-trivial terrains.

References

1. S. Avinash, A. Srivastava, A. Purohit, S. V. Shah and K. M. Krishna, "A Compliant Multi-Module Robot for Climbing Big Step-Like Obstacles," *Proceedings of the International Conference on Robotics and Automation*, IEEE (2014) pp. 3397–3402.
2. A. Siravuru, S. V. Shah and K. M. Krishna, "An optimal wheel-torque control on a compliant modular robot for wheel-slip minimization," *Robotica* **35**(2), 46–482 (2017).
3. S. H. Turlapati, M. Shah, P. Singamaneni, A. Siravuru, S. V. Shah and K. M. Krishna, "Stair Climbing Using a Compliant Modular Robot," *Proceedings of the International Conference on Intelligent Robots and Systems* (2015).

4. D. Choi, J. Oh and J. Kim, "Analysis method of climbing stairs with the Rocker–Bogie mechanism," *J. Mech. Sci. Technol.* **27**(9), 2783–2788 (2013).
5. T. Estier, Y. Crausaz, B. Merminod, M. Lauria, R. Piguet and R. Siegwart, "An Innovative Space Rover with Extended Climbing Abilities," *Proceedings of the 4th International Conference and Exposition on Robotics for Challenging Situations and Environments* (2000).
6. M. Lauria, Y. Piguet and R. Siegwart, "Octopus: An Autonomous Wheeled Climbing Robot," *Proceedings of the International Conference on Climbing and Walking Robots* (2002) pp. 315–322.
7. M. Eich, F. Grimminger, S. Bosse, D. Spenneberg and F. Kirchner, "Asguard: A Hybrid-Wheel Security and Sar-Robot Using Bio-Inspired Locomotion for Rough Terrain," *Proceedings of the International Workshop on Robotics for Risky Interventions & Surveillance of Environment*, Benicàssim, Spain (2008).
8. H. Komura, H. Yamada, S. Hirose, G. Endo and K. Suzumori, "Study of Swing-Grouser Wheel: A Wheel for Climbing High Steps, Even in Low Friction Environment," *Proceedings of the International Conference on Intelligent Robots and Systems*, IEEE (2015) pp. 4159–4164.
9. E. Z. Moore, D. Campbell, F. Grimminger and M. Buehler, "Reliable Stair Climbing in the Simple Hexapod'rhex'," *Proceedings of the International Conference on Robotics and Automation*, vol. 3, IEEE (2002) pp. 2222–2227.
10. J. B. Jeans and D. Hong, "Impass: Intelligent Mobility Platform with Active Spoke System," *Proceedings of the International Conference on Robotics and Automation*, IEEE (2009) pp. 1605–1606.
11. S. D. Herbert, A. Drenner and N. Papanikolopoulos, "Loper: A Quadruped-Hybrid Stair Climbing Robot," *Proceedings of the International Conference on Robotics and Automation*, IEEE (2008) pp. 799–804.
12. P. Ben-Tzvi, S. Ito and A. A. Goldenberg, "A mobile robot with autonomous climbing and descending of stairs," *Robotica* **27**(2), 171–188 (2009).
13. N. Senthilkumar, T. Tamizharasan and V. Anandakrishnan, "Experimental investigation and performance analysis of cemented carbide inserts of different geometries using Taguchi based Grey relational analysis," *Measurement* **58**, 520–536 (2014).
14. E. Z. Uporabo and Podlagi, "Multi-objective optimization of the cutting forces in turning operations using the Grey-based Taguchi method," *Mater. Tehnol.* **45**(2), 105–110 (2011).
15. G. Kibria, B. Doloi and B. Bhattacharyya, "Experimental investigation and multi-objective optimization of Nd:YAG laser micro-turning process of alumina ceramic using orthogonal array and Grey relational analysis," *Opt. Laser Technol.* **48**, 16–27 (2013).
16. Y. Kuo, T. Yang and G. Huang, "The use of Grey relational analysis in solving multiple attribute decision-making problems," *Comput. Ind. Eng.* **55**(1), 80–93 (2008).
17. H. Kalani, A. Akbarzadeh and H. Bahrami, "Application of statistical techniques in modeling and optimization of a snake robot," *Robotica* **31**(4), 62–641 (2013).
18. International Code Council, *International Building Code 2015*. (ICC, Country Club Hills, I, 2014).
19. R. T. Schroer, M. J. Boggess, R. J. Bachmann, R. D. Quinn and R. E. Ritzmann, "Comparing Cockroach and Whegs Robot Body Motions," *Proceedings of the International Conference on Robotics and Automation*, vol. 4, IEEE (2004) pp. 3288–3293.
20. G. S. Peace, *Taguchi Methods: A Hands-On Approach* (Addison-Wesley Publishing Company, Inc., Boston, MA, USA, 1993).
21. J.-L. Deng, "Introduction to Grey system theory," *J. Grey Syst.* **1**(1), 1–24 (1989).
22. M. Prado, A. Simón, A. Pérez and F. Ezquerro, "Effects of terrain irregularities on wheeled mobile robot," *Robotica* **21**(2), 143–152 (Mar. 2003).
23. B. K. Rout and R. K. Mittal, "Tolerance design of robot parameters using Taguchi method," *Mech. Syst. Signal Process.* **20**(8), 1832–1852 (2006).
24. D. Kim, H. Hong, H. S. Kim and J. Kim, "Optimal design and kinetic analysis of a stair-climbing mobile robot with Rocker–Bogie mechanism," *Mech. Mach. Theory* **50**, 90–108 (2012).
25. Y. Lee, Y. Han, C. C. Iuraşcu and F. C. Park, "Simulation-based actuator selection for redundantly actuated robot mechanisms," *J. Robot. Syst.* **19**(8), 379–390 (2002).
26. G. R. Iversen and H. Norpoth, *Analysis of Variance*, vol. 1 (SAGE Publications, Inc., Thousand Oaks, CA, USA, 1987).

Appendix: Spring stiffness calculation

The optimization formulation to solve for the spring stiffness values of the joints of the modular robot while climbing stairs primarily builds on quasi-static analysis of the robot.[3] The stair-climbing problem was divided into key phases that the robot undergoes, and the quasi-static equations for each phase were derived.[3] A locus method, proposed in our previous work,[3] was used to obtain the joint angles involved in each phase of stair climbing. Subsequently, the joint moment profiles were calculated corresponding to each phase by solving a constrained optimization problem subjected to static stability, friction cone and motor torque constraints. A linear fitting was then performed to approximate the spring stiffness from the joint moment profiles plotted against joint angles. The feasibility of this optimization problem per phase is valid unless there is an abrupt phase change. To avoid this, we also performed the quasi-static analysis of the robot as it climbed the sharp edge as an

interim phase. However, such an analysis yielded no significant results that contributed to the change in spring stiffness values. The quality of the solution, therefore, is preserved for the functional range of stair climbing. Extensive experimental results were also presented in ref. [3] to validate the same.

The above is summarized in the following five-step process:

- Step 1: Determining the joint angle profiles from the locus method, as the robot is imagined to climb stairs.
- Step 2: Using these joint angle profiles to determine unique configurations the robot undergoes as it climbs.
- Step 3: Deriving quasi-static equations for equilibrium at each of these configurations.
- Step 4: Carrying out numerical optimization to determine the optimal torque profile with the quasi-statics as the constraints and the joint angle profiles as the inputs in an iterative fashion.
- Step 5: Linear least squares fitting to find the optimal spring stiffness that can approximate the torque profile obtained in Step 4.